Applied Catalysis B: Environmental 85 (2008) 40–47

Contents lists available at ScienceDirect

Applied Catalysis B: Environmental

journal homepage: www.elsevier.com/locate/apcatb

Optimization of the $MnCeO_x$ system for the catalytic wet oxidation of phenol with oxygen (CWAO)

Francesco Arena [a,b,*], Giuseppe Trunfio [a], Jacopo Negro [a], Lorenzo Spadaro [b]

[a] Dipartimento di Chimica Industriale e Ingegneria dei Materiali, Università degli Studi di Messina, Salita Sperone 31 c.p. 29, I-98166 S. Agata (Messina), Italy
[b] Istituto CNR-ITAE "Nicola Giordano", Salita S. Lucia 5, I-98126 S. Lucia (Messina), Italy

ARTICLE INFO

Article history:
Received 8 May 2008
Received in revised form 19 June 2008
Accepted 21 June 2008
Available online 1 July 2008

Keywords:
$MnCeO_x$ catalyst
Preparation method
Redox-precipitation
Composition
Textural properties
Molecular dispersion
Reducibility
Catalytic activity
CWAO
Phenol

ABSTRACT

A class of $MnCeO_x$ catalysts has been synthesized *via* the new *redox-precipitation* route in alternative to the conventional co-precipitation technique. The effects of preparation method, composition and calcination temperature on catalyst texture, dispersion and reduction pattern properties have been addressed. Redox-precipitated systems exhibit high surface area (SA, 120–170 m^2/g), large pore volume (PV, 0.4–0.5 cm^3/g) and a "narrow" pore size distribution (PSD) in a wide range of the Mn/Ce ratio (1/3–3/1). A quasi-*molecular* dispersion markedly improves *oxide-support* interactions and reducibility of the active phase. Redox-precipitated systems show a superior performance in the catalytic wet oxidation of phenol with oxygen (CWAO) at 373 K in terms of substrate and total organic carbon (TOC) elimination and mineralization (i.e., CO_2 formation) selectivity. Carbon mass-balance from TG-DSC data of used catalysts and CO_2 selectivity values signal that the CWAO of phenol proceeds *via* a L–H reaction path, the oxidation of C-containing species being the *rate limiting step* (*r.l.s.*). Then, an optimum average pore diameter (APD, 10–15 nm) enhances the rate of the adsorption step, while a straight relation between CO_2 selectivity and reducibility prove that dispersion and redox properties of the active phase control the mineralization activity of the $MnCeO_x$ system.

1. Introduction

The increasing worldwide demand for human life's essentials water supply is pressing a great scientific and technological concern on new technologies for water purification, as reclaim and recycle of wastewater and sewage is compulsory to reduce the request of agricultural and industrial activities, both accounting to ca. 92% of global water consumption [1–4]. Disposal of waste streams containing toxic organic pollutants generated by many industrial processes also deserves a proper concern to accomplish more and more stringent legislative targets for the safeguard of natural resources and environment [1–4]. In this context, as one of the available technologies, the heterogeneous catalytic wet air oxidation (CWAO) is a very promising route to attain an effective mineralization of many non-biodegradable pollutants and noxious organic substrates that are toxic and/or refractory to conventional biological treatments [2–4]. Nevertheless, noble-metal catalyst formulations in concomitance with high process temperatures (>473 K) render current CWAO technologies economically unfavourable for routine applications [2–4]. Then, the development of efficient, robust and low-cost catalysts prompted in the last years a major research interest on the CWAO pattern of oxide systems, mostly Cu [5,6] and Mn [2–4,7–14] ones. Claimed as very effective CWAO catalysts towards various model compounds, however we documented the failure of Cu catalysts due to the extensive leaching of the active phase, driving mostly a homogeneous reaction path [5,6]. Therefore, $MnCeO_x$ systems remain the sole reliable alternative with a performance comparable or superior to that of noble-metals [2–4,7–15]. However, their CWAO performance is decisively affected by textural, structural and redox properties [4,7–15], deserving proper preparation routes [7–9,13,14] and composition adjustments [4,10–13,15,19] for catalyst optimization. Indeed, Abecassis-Wolfovich et al. related the activity of *nanocasted* systems in the CWAO of chlorophenols to very high surface area and stabilization of the Mn_5O_8 phase [8], according to our previous mechanistic findings proving the crucial role of textural and redox properties on the CWAO activity of the $MnCeO_x$ system [7,13]. Then, we preliminarily documented a

* Corresponding author at: Dipartimento di Chimica Industriale e Ingegneria dei Materiali, Università degli Studi di Messina, Salita Sperone 31 c.p. 29, I-98166 S. Agata (Messina), Italy. Tel.: +39 090 676 56 06; fax: +39 090 391 518.
E-mail address: Francesco.Arena@unime.it (F. Arena).

0926-3373/$ – see front matter © 2008 Elsevier B.V. All rights reserved.
doi:10.1016/j.apcatb.2008.06.020

superior performance in the CWAO of phenol of the $MnCeO_x$ catalyst (Mn/Ce, 1) synthesized via the new *redox-precipitation* route in comparison to a "conventional" co-precipitated system [7,16,17].

Therefore, this paper addresses a systematic investigation of the effects of preparation method, composition and calcination temperature on textural, redox and catalytic properties of $MnCeO_x$ systems obtained via redox-precipitation and co-precipitation routes. High surface area (SA), a uniform pore size distribution (PSD) and quasi-*molecular* dispersion of the active phase in a wide range of the Mn/Ce ratio (1/3–3/1) strongly enhances the reactivity of redox-precipitated systems in the CWAO of phenol in comparison to co-precipitated ones. In agreement with previous mechanistic evidences [7], basic structure–activity relationships constitute a scientific background to catalyst design and optimization for the CWAO process.

2. Experimental

2.1. Catalyst preparation

$MnCeO_x$ catalysts with Mn/Ce atomic ratio (i.e., x/y) ranging between 1/3 and 3/1 were prepared *via* the *redox-precipitation* route, consisting in the titration at constant pH (8.0 ± 0.2 by addition of KOH) of the $KMnO_4$ precursor with a solution of Ce^{3+} and Mn^{2+} nitrates [7,16,17]. After titration, catalysts were filtered, washed, dried at 373 K (16 h) and further calcined (6 h) in air at 673 K (MxCy-R4). An aliquot of the M1C1-R sample was used in the dried form (M1C1-R), while another one was calcined at 873 K (M1C1-R6). Moreover, the influence of the alkaline agent was evaluated using LiOH (M1C1-R4L) and NH_4OH (M1C1-R4N) instead of KOH for the synthesis of M1C1-R4 samples. A $MnCeO_x$ sample with Mn/Ce equal to 1, prepared *via* co-precipitation of $MnCl_2$ and $CeCl_3$ (M1C1-P4) precursors, was taken as reference [10,15–17]. The list of catalysts with the relative notation and main physico-chemical properties is given in Table 1.

2.2. Catalyst characterization

Surface area and pore size distributions were obtained from N_2 adsorption–desorption isotherms (77 K) using a ASAP 2010 (*Micromeritics Instruments*) static adsorption device. Isotherms were elaborated by the BET method for SA calculation, while micro and mesopore distributions were determined by Horvath-Kavazoe and BJH methods, respectively.

X-ray photoelectron spectroscopy (XPS) data were obtained using a *Physical Electronics GMBH PHI 5800-01* spectrometer operating with a monochromatized Al Kα radiation with a power beam of 350 W and pass energy of 11.0 eV.

Temperature programmed reduction (TPR) measurements of untreated catalyst samples (ca. 30 mg) in the range 293–773 K were carried out using a 6% H_2/Ar mixture flowing at 60 stp mL min^{-1} into a linear microreactor (d_{int}, 4 mm) heated at the rate of 12 K min^{-1}. The H_2 consumption was detected by a TCD quantitatively calibrated by known amounts of CuO.

Thermogravimetric (TG-DSC) analysis of the used samples was performed in static air with a heating rate of 5 K/min, using a *Netzsch Simultaneous Thermal Analysis Instrument* (*STA 409C*).

2.3. Catalyst testing

Activity measurements in the CWAO of phenol at 373 K were performed in semi-batch mode using a 0.25 L stirred (≈1000 rpm) autoclave loaded with a 0.14 L volume of bi-distilled water and a catalyst sample (d_p, 20 μm) of 0.75 g, fed with a pure oxygen flow at the rate of 0.1 stp L min^{-1} (P_R, 1.0 MPa; P_{O_2}, 0.9 MPa). Two consecutive reaction tests of 1 h were run on each catalyst by injecting into reactor a 10 mL aqueous solution of phenol, corresponding to an initial concentration of 1000 ± 50 ppm (0.15 g/0.15 L), at the time 0 and after 1 h, respectively. Under such conditions intraparticle mass transfer resistances were negligible according to the Weisz-Prater criterion [7]. Liquid reaction samples were analyzed with respect to pH, phenol (*Dionex* HPLC), Total Organic Carbon (*Shimadzu TOC Analyser*) and Mn concentration (AAS). In addition, the mineralization selectivity (i.e., CO_2 formation) was probed by bubbling the outlet gaseous stream in a stirred $Ba(OH)_2$ solution and weighing the precipitated $BaCO_3$ after filtration, washing and drying at 373 K (16 h) [7].

3. Results and discussion

3.1. Effects of synthesis, composition and calcination temperature on textural, structural and redox properties

The summary of physico-chemical properties shows that redox-precipitated catalysts are characterized by higher surface area values than co-precipitated system in the whole range of the Mn/Ce ratio (Table 1). Although we previously argued the advantage of the disclosed route in forwarding an unchanging solid architecture [16,17], the changes in SA and average pore diameter (APD) with the Mn/Ce ratio actually disclose a *composition-effect* on the morphology of the redox-precipitated system that is shown in Fig. 1. A linear decrease in SA and a regular growth in the APD are in fact diagnostic of a slight negative influence of the MnO_x loading on the surface exposure of the redox-precipitated system [4,10,18–20]. At variance, the effects of composition on the texture of the co-precipitated catalysts are less systematic and predictable [4,7,10,11,13,15,18–20]. Fig. 1, comparing also litera-

Table 1
Notation and main physico-chemical properties of the catalysts calcined at 673 K

Catalyst	Prep. meth.	Mn/Ce[a]		[Mn] (wt%)	SA (m^2/g)	PV (cm^3/g)	APD[b] (nm)	Mn/Ce[c]
		Des.	Exp.					
M1C3-R4	Redox-precipitation	0.33	0.34	9.3	168	0.28	3.8	0.58
M3C4-R4	Redox-precipitation	0.75	0.71	16.7	169	0.47	7.2	1.00
M1C1-R4	Redox-precipitation	1.00	0.95	20.5	159	0.49	11.7	1.33
M3C2-R4	Redox-precipitation	1.50	1.44	26.6	157	0.45	14.3	1.80
M2C1-R4	Redox-precipitation	2.00	2.12	32.7	140	0.50	16.7	2.69
M3C1-R4	Redox-precipitation	3.00	2.76	36.8	117	0.46	18.3	3.42
M1C1-P4	Co-precipitation	1.00	1.00	21.2	101	0.24	9.4	0.40

[a] Mn/Ce atomic ratio from design and XRF measurements, respectively.
[b] Average pore diameter.
[c] Surface Mn/Ce atomic ratio from XPS measurements.

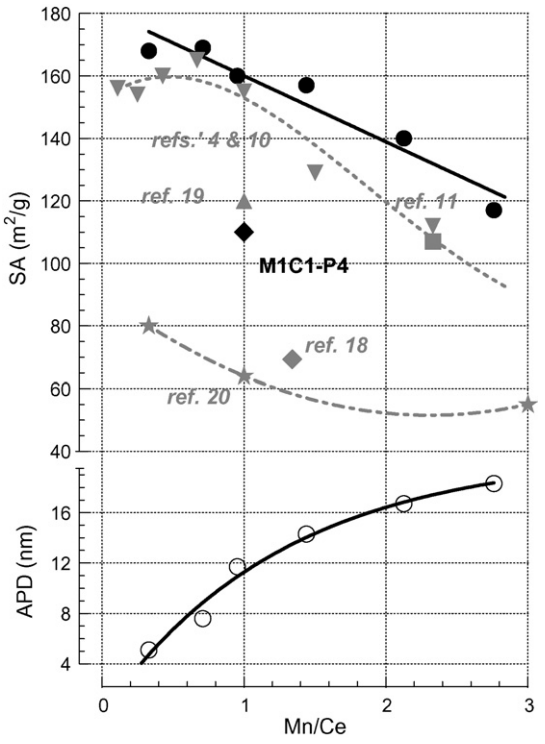

Fig. 1. Effect of the Mn/Ce ratio on surface area (SA) and average pore diameter (APD) of redox-precipitated catalysts calcined at 673 K.

ture data of catalysts obtained via co-precipitation and calcined between 623 and 773 K, show indeed a higher variability in SA values and two differently decreasing relationships for catalysts obtained from chlorides [4,10] and nitrates [20], respectively, diagnostic of the marked influence of precursors on the morphology of the final catalyst [7,10,16,17,19,20]. Whereas, slight differences (<10%) in SA, APD and pore volume (PV) of the M1C1-R4 system, with varying the $KMnO_4$ concentration (5–10 g/L) or type of alkaline agent used for the synthesis (Table 2), match the occurrence of an unchanging reaction path between MnO_4^- and Ce^{3+}–Mn^{2+} precursors accounting for the superior reproducibility ensured by the redox-precipitation route [16,17].

The pore size distribution of the studied catalysts (Fig. 2) sheds further lights into the effects of preparation method and composition on the texture of the $MnCeO_x$ system. In agreement with SA and APD data, Fig. 2A outlines marked differences in the porous structure of M1C1-R4 and M1C1-P4 catalysts, while redox-precipitated catalysts feature a regular PSD irrespective of composition (Fig. 2B) and synthesis parameters (Fig. 2A). Apart from a slight contribution (10–20%) of micropores, all redox-precipitated systems display in fact "narrow" *Gaussian*-shaped PSD's, whose maximum shifts from ca. 4 to 11 nm upon the Mn/Ce ratio rises from 1/3 to 2/1. All the systems with analogous composition (e.g., M1C1-R4. M1C1-R4L and M1C1-R4N) feature a quite similar PSD (Fig. 2A), while the different shape of the PSD of the M3C1-R4 sample mirrors the above *composition-effect* on catalyst texture, since an abrupt upward shift of the PSD allows the descending branch of the Gaussian curve falling out of the mesopore range (Fig. 2B). These regular trends also in the porous structure depend upon the direct formation of nanosized (5–10 nm) $MnCeO_x$ composite oxide particles in the redox-precipitation process and the consequent lack of precursors-decomposition and phase-reconstruction phenomena in the calcination step [7,16,17]. The substantial reproducibility of textural properties of the redox-precipitated system result also in constant pore volume values (0.4–0.5 cm^3/g) that are some two times larger than that of the co-precipitated sample (0.24 cm^3/g) [7,13,16–20].

Table 2
Influence of synthesis parameters on the textural properties of the M1C1-R4 system

Catalyst	Alkaline agent	Mn/Ce[a]	Tcalc (K)	SA (m^2/g)	PV (cm^3/g)	APD[b] (nm)	Mn/Ce[c]
M1C1-R4	KOH	0.95	673	154	0.49	11.7	1.33
M1C1-R4*	KOH[d]	0.97	673	171	0.43	11.1	1.29
M1C1-R4N	NH_4OH	0.89	673	166	0.43	6.5	1.21
M1C1-R4L	LiOH	0.98	673	163	0.45	9.3	1.30

[a] Mn/Ce atomic ratio from XRF measurements.
[b] Average pore diameter.
[c] Surface Mn/Ce atomic ratio from XPS measurements.
[d] $KMnO_4$ concentration ≈5 g/L.

The different structure of the $MnCeO_x$ system induced by the preparation method is even more evident from the active phase dispersion data [16,17] that is probed by the XPS Mn/Ce ratios in Tables 1 and 2. A surface ratio larger than bulk signals in fact a surface MnO_x enrichment that is a characteristic of the disclosed route [16,17]. In fact, comparing these figures with literature data of co-precipitated systems [4,10,18] as a function of the relative bulk composition, two straight-line relationships with slope values of ca. 1.2 and 0.5 are obtained (Fig. 3). These findings confirm that the redox-precipitated system is characterized by a uniform, *molecular-like*, dispersion of Mn ions across the ceria matrix at any Mn/Ce ratio and that the accessibility of the active phase is not substantially influenced by clustering-sintering phenomena for calcination temperatures lower than 873 K [16,17]. At variance, a three times lower surface Mn/Ce ratio of co-precipitated samples mirrors a considerably lower surface availability of the active phase due to an extensive clustering and formation of crystalline MnO_x species [4,10,15–20].

The influence of the calcination temperature on the surface texture of the M1C1-R system is shown in Fig. 4, comparing the SA, PV and APD (Fig. 4A) and PSD (Fig. 4B) of samples calcined in the range 373–873 K. As expected, a rise in the calcination temperature causes a progressive SA decay from 215 (M1C1-R) to 90 m^2/g (M1C1-R6), while slight changes in PV reflect a growth of APD almost specular to the SA decay. An upward shift and broadening in the PSD, consistent with the growth in APD, signals the closer packing induced by higher calcination temperatures leading to the progressive closure of small sized pores [16].

The redox properties of the studied catalysts were probed by TPR analysis in the range 293–773 K, the spectra being shown in Fig. 5 with reference to the effects of the Mn/Ce ratio (A), preparation method (B) and calcination temperature (C), while Table 3 lists the values of onset ($T_{o,red}$) and maximum reduction temperature (T_M) and the extent of H_2 consumption. The TPR profiles of the differently loaded redox-precipitated catalysts (Fig. 5A) consist of a broad band spanned in the range 373–673 K, with poorly resolved maxima at ca. 530 and 590 K, with a shoulder at ca. 673 K more evident on the M1C3-R4 sample. An increasing intensity of the signal at lower temperatures accounts for a regularly rising amount of H_2 consumption with the Mn loading, though the H_2/Mn ratio follows an opposite decreasing trend (Table 3). These qualitative features mostly indicate the reduction of "isolated" Mn ions embedded into the ceria matrix (T_M, 530 K) and small MnO_2 clusters (T_M, 590 K), promoting the overall reducibility of the system at low temperature [7,16,17]. Indeed, inspecting the influence of preparation method (Fig. 5B), the co-precipitated M1C1-P4 system shows a fairly different profile shifted to higher temperature ($T_{o,red}$, 400 K). Two resolved components centered at 585 and 675 K, attributable to reduction of crystalline MnO_2 and Mn_2O_3 species, respectively [7,16,17,21]

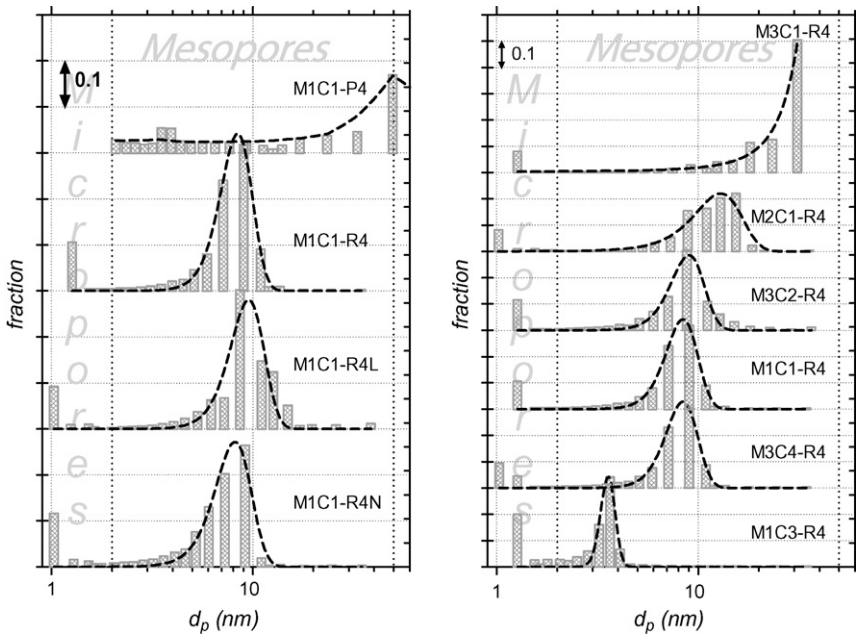

Fig. 2. (A) Effect of the preparation method on the pore size distribution (PSD) of M1C1-Y4 catalysts calcined at 673 K; (B) Effect of the Mn/Ce ratio on the PSD of redox-precipitated catalysts calcined at 673 K.

account for an extent of hydrogen consumption that is ca. 20% lower than that of the M1C1-R4 sample (Table 3). Whereas, M1C1-R4 samples synthesized using different alkaline agents display similar spectra, only a slightly lower H_2 consumption being recorded for the M1C1-R4L sample (Table 3). Then, redox-precipitated catalysts miss the component at ca. 670 K of crystalline Mn_2O_3 particles, while the peak of "isolated" Mn^{4+} ions is nearly absent in the spectrum of the M1C1-P4 system because of the much lower dispersion of the active phase [7,16,17]. Finally, the spectra of the M1C1-R system calcined at different temperatures (Fig. 5C) displays some changes in the reduction pattern of the M1C1-R6 sample, consistent with the above assignation. Indeed, the SA decay of the latter sample (Fig. 4A) is associated with a structural rearrangement leading to clustering of MnO_2 and CeO_2 phases [17]. Therefore, the sintering of "isolated" Mn moieties into crystalline MnO_2 clusters accounts for the almost complete disappearance of the component at 535 K.

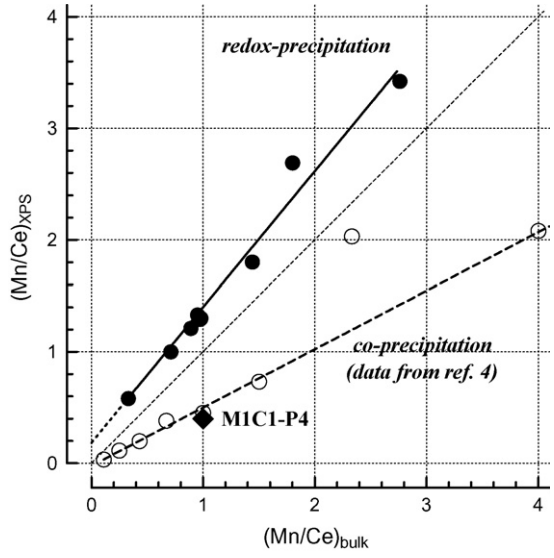

Fig. 3. Surface XPS Mn/Ce ratio of redox-precipitated and co-precipitated catalysts (values taken from Refs. [4,10]) as a function of the bulk composition.

3.2. Activity pattern in the CWAO of phenol and structure–activity relationships

Phenol CWAO activity data at 373 K of $MnCeO_x$ catalysts (Mn/Ce, 1) prepared *via* redox-precipitation (M1C1-R4) and co-precipitation (M1C1-P4) routes in two consecutive runs are shown in Fig. 6. For the sake of clarity, phenol and TOC concentration (Fig. 6A) and conversion and pH of the reacting solution (Fig. 6B) *vs.* reaction time are shown. The M1C1-R4 catalyst features a very high CWAO performance that ensures a complete (>95%) elimination of phenol and TOC in both first and second runs after ca. 15 and 45 min, respectively. The M1C1-P4 system is considerably less active as in the first run it attains a complete elimination of phenol and TOC only after 1 h, and a partial removal of phenol (ca. 85%) and TOC (ca. 75%) in the second run. Moreover, an almost instantaneous pH decrease to a value of 4.2 is recorded with the M1C1-R4 catalyst, while for the latter one a final pH value of 4.9 is recorded after ca. 30 min. These data, indicative of the incipient oxidation of the substrate into carboxylic acids such as formic, oxalic and acetic ones [2–7,10–15], preliminarily signal a higher oxidation strength of the redox-precipitated system (see *infra*). However, despite of the acidic pH, in both cases the extent of leaching was negligible with final (i.e., after 2 h) concentration values of Mn ions in the reacting solution lower than 1 ppm, corresponding to less than 0.1% of the overall manganese load [7].

The effects of the Mn/Ce ratio, synthesis parameters and calcination temperature on the CWAO activity of the redox-precipitated system are summarized in Table 4 in terms of time required for total phenol ($t_{X,\ PhOH}$) and TOC ($t_{X,\ TOC}$) removal, half-life time of phenol ($t_{1/2,\ PhOH}$) and TOC ($t_{1/2,\ TOC}$) and final pH value. All the catalysts feature a high CWAO activity, ensuring a complete removal of both substrate and TOC in the first run in a time comprised between 15 and 60 min. In the second reaction cycle an incipient deactivation is evident from lower rates of phenol and TOC removal, which in most cases is partial (Table 4). Since all

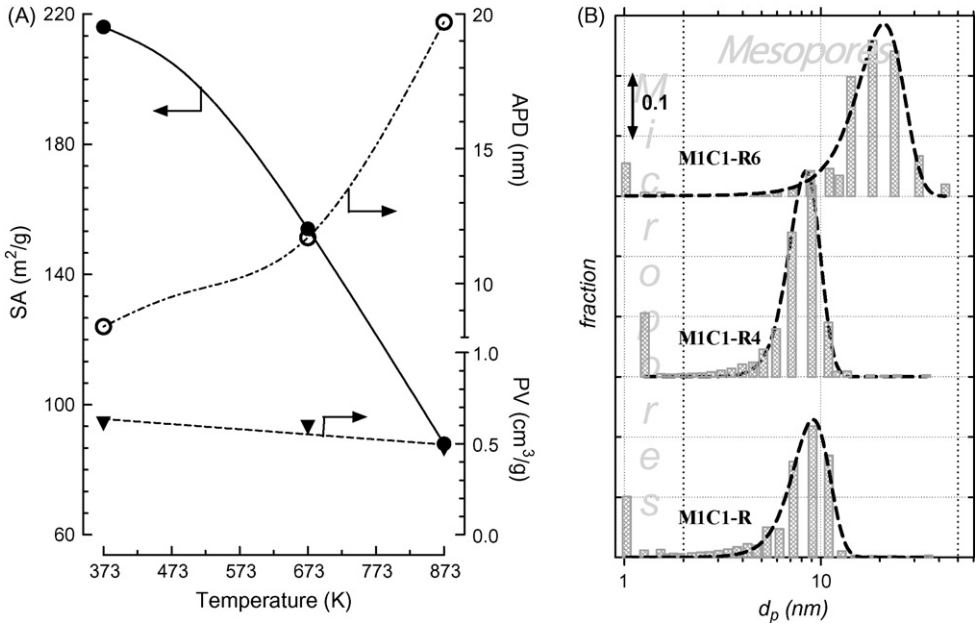

Fig. 4. (A) Effect of the calcination temperature on surface area, average pore diameter and pore volume (PV) of the M1C1-R catalyst. (B) Effect of the calcination temperature on PSD of the M1C1-R catalyst.

conversion data satisfactorily match first-order reaction kinetics (Fig. 6B)

$$-\frac{dC_X}{dt} = k_X C_X[\text{Cat}]$$

a comparison of the various catalysts can be made on the basis of the constants of phenol (k_{phen}) and TOC (k_{TOC}) removal, also listed in Table 4. The kinetic constants of the M1C1-P4 sample in the first reaction cycle (ca. 0.9–1.1 L g_{cat}^{-1} h^{-1}) well compares with the values (0.5–1.2 L g_{cat}^{-1} h^{-1}) quoted by Abecassis-Wolfovich et al. for similar co-precipitated $MnCeO_x$ systems [15], although these are considerably lower than those of redox-precipitated catalysts (2–3 L g_{cat}^{-1} h^{-1}) with Mn/Ce > 1/3. Indeed, a *composition-effect* on the CWAO pattern of the redox-precipitated system emerges from the kinetic constants of phenol and TOC removal, depicting peculiar volcano-shaped relationships as a function of the Mn/Ce ratio with maximum at a value of 1 (Fig. 7), similar to that found for co-precipitated systems [4,10].

The CWAO data of the M1C1-R4 system obtained using various types of bases indicate that the catalyst prepared using LiOH (M1C1-R4L) features an activity level analogous to that of the M1C1-R4 sample both in the first and second runs, whilst that obtained using NH_4OH (M1C1-R4N) is considerably less active, mostly in the second reaction cycle when a ca. 50% plateau in the conversion of phenol and TOC is attained (Table 4).

Therefore, although Fig. 7 seems to point to an optimum surface composition ensuring a higher surface chemical affinity for the substrate [4,10] previous mechanistic evidences, showing that the removal of substrate and TOC is due to surface adsorption [4,7,10,13,15,22], suggest that also the textural properties can play a basic influence on the CWAO pattern of the $MnCeO_x$ system. Then, considering the regular decrease in SA (Fig. 1), the minor

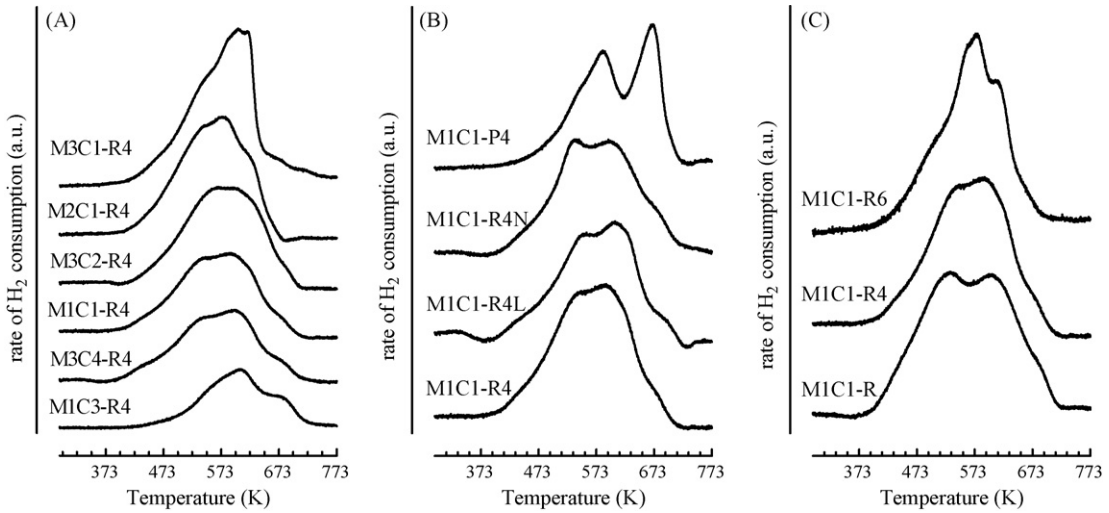

Fig. 5. (A) Influence of the Mn/Ce ratio on the TPR profiles of MxCy-R4 catalysts. (B) Effect of the preparation method on the TPR profile of the M1C1-Y4 system; (C) Effect of the calcination temperature on the TPR profile of the M1C1-R catalyst.

Table 3
TPR data of $MnCeO_x$ catalysts

Catalyst	$T_{o,red}$ (K)	T_{M1} (K)	T_{M2} (K)	T_{M3} (K)	H_2 consumption	
					mmol/g_{cat}	H_2/Mn
M1C3-R4	390	–	599	670	1.94	1.16
M3C4-R4	375	529	599	–	2.95	0.93
M1C1-R4	365	534	591	–	3.27	0.85
M3C2-R4	365	546	597	–	3.78	0.77
M2C1-R4	375	539	589	–	4.60	0.79
M3C1-R4	383	547	605	–	5.46	0.79
M1C1-P4	400	–	585	672	2.71	0.67
M1C1-R4L	375	541	597	–	2.58	0.76
M1C1-R4N	375	534	591	–	3.08	0.86
M1C1-R	365	517	598	–	3.30	0.86
M1C1-R6	383	–	575	612	2.87	0.74

differences in PV (Tables 1 and 2) and the different activity level of catalysts with analogous composition (e.g., M1C1-R4, M1C1-R4L and M1C1-R4N) and SA (154–171 m^2/g), it can be inferred that the porous structure likely plays a fundamental influence on the CWAO pattern of the redox-precipitated system [22]. In fact, plotting all the values of k_{PhOH} and k_{TOC} of catalysts calcined at 673 K against the APD, an optimum value in the range 10–15 nm ensuring higher phenol and TOC adsorption rates is found (Fig. 8). Due to small intraparticle diffusion rates, this relationship suggests that small pores hinder the phenol adsorption, though analogous values of constant of phenol and TOC removal signal a minor tendency of catalysts on the left side of the maximum to release reaction intermediates. On the other hand, APD's larger than 10–15 nm allow an easier adsorption/desorption of phenol and, mostly, of light intermediates accounting for the stronger decrease in k_{TOC} (Fig. 8). The different porous structure also accounts for a steeper decrease of k_{phen} in the second reaction run on the M1C1-R4 system in comparison to the M1C1-P4 one (Table 4). In particular, the strong decrease (ca. 60%) in both k_{phen} and k_{TOC} can be attributed to the homogeneously tiny size of the porous network of the M1C1-R4 catalyst (Fig. 2) hindering phenol adsorption in the second run. Whereas, the slight relative decrease in k_{phen} of the M1C1-P4 sample (ca. 30%) is likely attributable to the overwhelming presence of large pores (Fig. 2A) allowing minor changes in the relative phenol adsorption capacity. Anyhow, a decrease in k_{TOC} comparable with that of the counterpart M1C1-R4 system (ca. 55%), indicates also an extensive release of reaction intermediates in the solution, confirming the much lower CWAO efficiency of the co-precipitated sample [7,13,14].

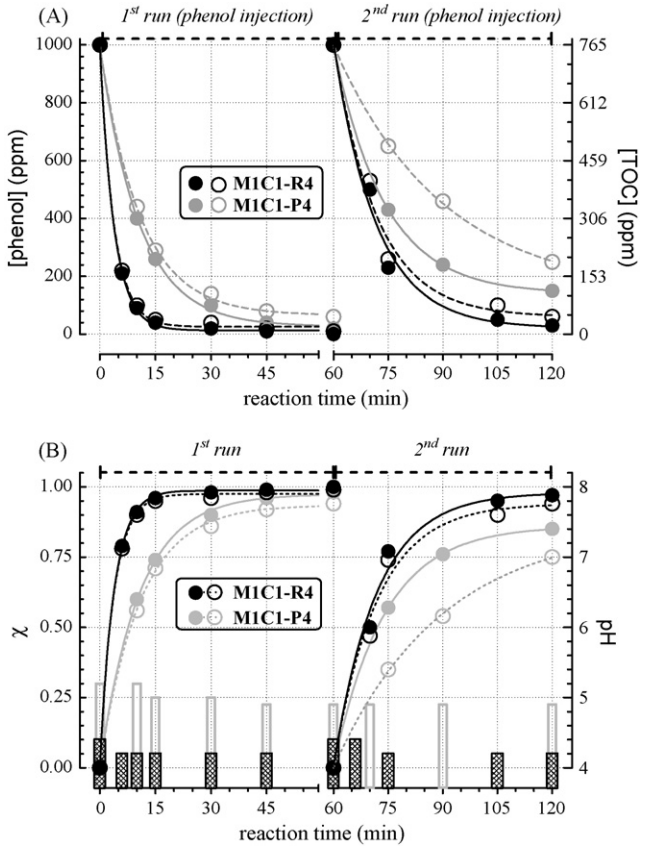

Fig. 6. CWAO activity data (T, 373 K; P, 1.0 MPa) of the M1C1-R4 and M1C1-P4 catalysts. (A) Phenol (full symbols) and TOC (open symbols) concentration *vs.* reaction time. (B) Phenol (full symbols) and TOC (open symbols) conversion and pH (bars) of the reacting solution *vs.* reaction time.

According to the fact that a calcination temperature in excess of 673 K significantly affects the structural and redox properties of the M1C1-R system [17], the M1C1-R and M1C1-R4 catalysts exhibit a similar CWAO activity that is considerably better than that of the M1C1-R6 system (Table 4). The relative kinetic

Table 4
CWAO of phenol at 373 K

Catalyst	First cycle				Second cycle				pH	First cycle		Second cycle	
	$t_{X,PhOH}$[a] (min)	$t_{X,TOC}$[a] (min)	$t_{1/2,PhOH}$ (min)	$t_{1/2,TOC}$ (min)	$t_{X,PhOH}$[a] (min)	$t_{X,TOC}$[a] (min)	$t_{1/2,PhOH}$ (min)	$t_{1/2,TOC}$ (min)		k_{PhOH} (L g^{-1} h^{-1})	k_{TOC} (L g^{-1} h^{-1})	k_{PhOH} (L g^{-1} h^{-1})	k_{TOC} (L g^{-1} h^{-1})
M1C3-R4	45	50	6.9	7.4	>60 (51)	>60 (51)	60	60	4.3	1.2	1.2	0.7	0.7
M3C4-R4	30	40	4.7	5.1	>60 (94)	>60 (91)	11	11.9	4.2	1.8	1.6	0.8	0.8
M1C1-R4	15	20	2.6	2.6	45	>60 (92)	6.0	6.5	4.2	3.2	3.1	1.4	1.4
M3C2-R4	20	60	3.8	3.9	60	>60 (88)	4.3	4.5	4.3	2.2	2.2	1.9	1.5
M2C1-R4	25	30	3.9	3.9	50	>60 (89)	5.8	6.6	4.2	2.1	2.1	1.6	1.5
M3C1-R4	30	>60 (89)	3.6	5.1	>60 (94)	>60 (83)	5.0	9.1	5.3	2.0	1.2	1.6	1.2
M1C1-P4	45	>60 (94)	7.3	7.5	>60 (86)	>60 (76)	12	26.0	4.9	1.1	0.9	0.8	0.4
M1C1-R4L	15	25	3.6	3.9	40	>60 (93)	7.3	7.5	4.1	2.1	2.0	1.2	1.1
M1C1-R4N	30	30	4.8	5.0	>60 (58)	>60 (53)	13	15.7	4.1	1.3	1.2	0.7	0.6
M1C1-R	15	15	2.5	2.5	45	>60 (90)	6.6	6.7	4.2	3.3	3.1	1.3	1.1
M1C1-R6	30	30	6.0	6.3	>60 (93)	>60 (86)	8.3	8.7	4.9	1.4	1.3	0.9	0.8

Activity data of the studied catalysts: time of total (>95%) phenol and TOC conversion, half-life time of phenol and TOC, final pH value and *pseudo-first-order* kinetic constants of phenol and TOC removal.

[a] In all the cases of time for total (>95%) conversion exceeding 1 h, the final conversion value is reported between brackets.

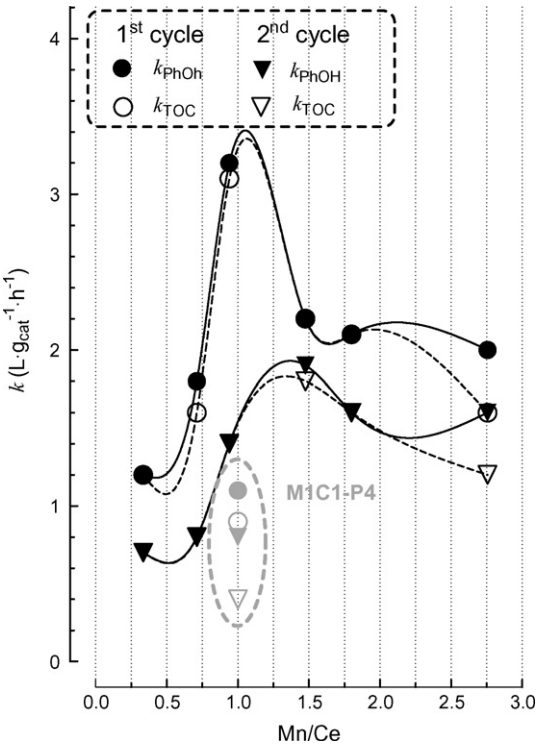

Fig. 7. Relationship between the kinetic constants of phenol and TOC conversion in the first and second reaction runs and Mn/Ce ratio of MxCy-R4 catalysts.

constants of phenol and TOC removal, comparable with those of the M1C1-P4 catalyst, mirror in this case the structural modifications leading to the aforesaid SA decay and broadening in PSD and APD (Fig. 3).

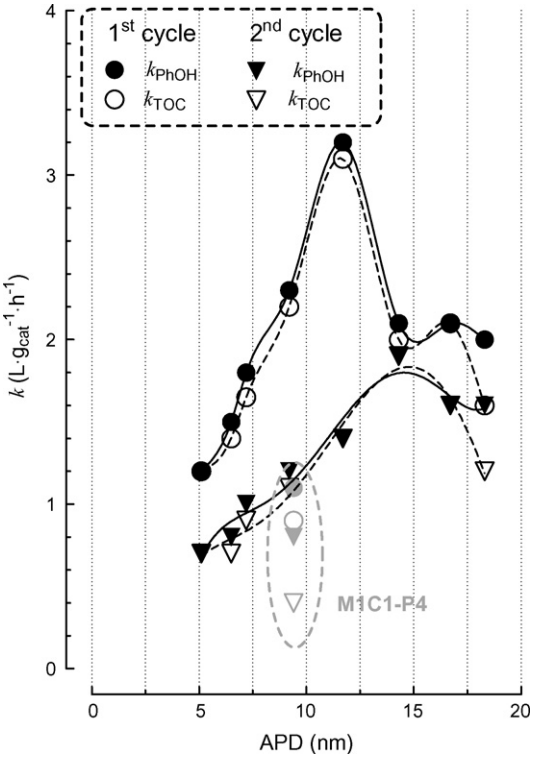

Fig. 8. Relationships between the kinetic constants of phenol and TOC conversion in the first and second reaction runs and average pore diameter of redox-precipitated catalysts calcined at 673K (see Table 4).

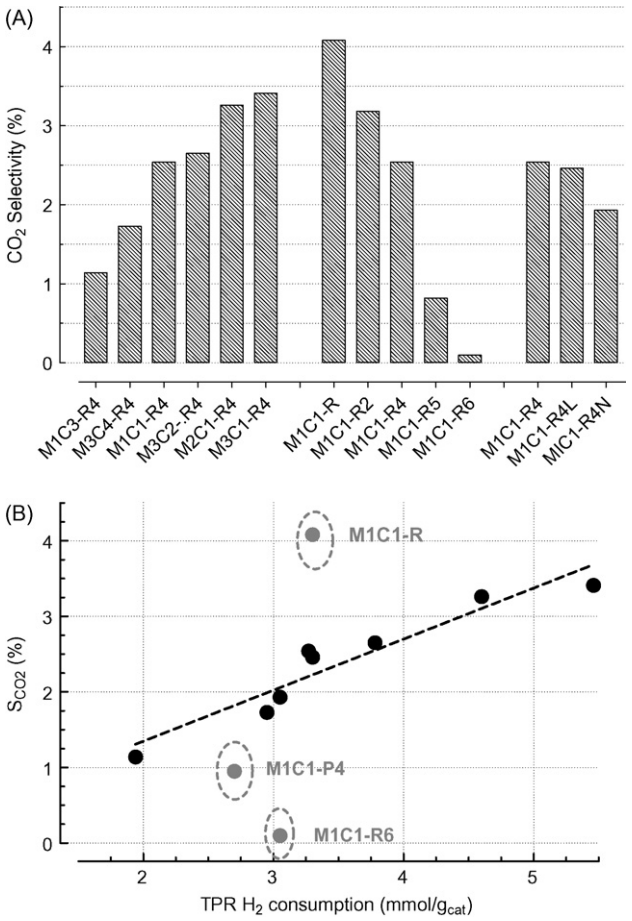

Fig. 9. (A) Final CO_2 selectivity of the various catalysts in the CWAO of phenol at 373 K. (B) Relationship between CO_2 selectivity values and extent of H_2 consumption (Table 3) of the various catalysts.

Finally, the CO_2 selectivity, true index of the mineralization activity [7,13–15], and carbon-mass balance deserve some specific considerations. Fig. 9A, comparing the mineralization selectivity of the various catalysts at the end of runs, show CO_2 selectivity values comprised between 0.1 (M1C1-R6) and 4% (M1C1-R), and an increasing trend with the Mn loading. These low CO_2 selectivity values confirm that the surface oxidation of C-containing species is the *rate-limiting step* [7,13–15] in comparison to the much faster adsorption step, generally taken as measure of the activity of heterogeneous CWAO catalysts [2–4,7,10,15,22]. In fact, we showed that phenol oxidation occurs in concomitance with the reduction of the active phase, due to the fact that electron-transfer from O to Mn ions (i.e., $Mn^{n+} - O^{2-} \rightarrow Mn^{(n-1)+} - O^{-}$) controls the formation of *electrophylic* oxygen species yielding total oxidation [23]. Thus, mechanistic evidences suggest the CO_2 selectivity is somewhat related to the redox behavior of the catalysts. Indeed, taking the H_2 consumption recorded by TPR measurements (Table 3) as a measure of the reducibility of the active phase, the CO_2 selectivity values result a straight-line function of this parameter (Fig. 9B). Only data of M1C1-P4, M1C1-R6 and M1C1-R catalysts show major deviations from this correlation because of the different dispersion and reducibility of the active phase. In fact, the M1C1-R6 and M1C1-P4 catalysts feature low CO_2 selectivity due to a low, if any, concentration of isolated Mn^{4+} ions while, at variance, the M1C1-R system enables the highest mineralization activity

owing to the largest concentration of that easily reducible species [16].

In agreement with above CO_2 selectivity values, then the TG-DSC analysis of the "used" catalysts provide weight-loss data between 25 and 29%, that accounted for a carbon-mass balance better than 95% [7].

4. Conclusions

The effects of synthesis, composition and calcination temperature on textural and redox properties of $MnCeO_x$ catalysts have been addressed.

Irrespective of the Mn/Ce ratio, the *redox-precipitation* route ensures large surface area, a uniform pore size distribution and a *monolayer* active phase dispersion, strongly promoting the performance of the system in the CWAO of phenol.

An optimum APD (10–15 nm) enables a superior efficiency in the elimination of phenol and TOC, while the mineralization efficiency relies on the redox properties of the system.

Structural, redox and catalytic features of redox-precipitated catalysts are slightly affected by calcination in the range 373–673 K, while at 873 K a deep structural rearrangement has a strongly negative impact on their CWAO performance.

A molecular-like oxide dispersion prompts an easy reduction of the active phase speeding-up the combustion of adsorbed intermediates, *rate-limiting step* of the CWAO of phenol.

References

[1] J. Kemsley, C&EN 28 (January 2008) 71.
[2] S. Imamura, in: A. Trovarelli (Ed.), Catalysis by Ceria and Related Materials, vol. 14, Imperial College Press, London, UK, 2002, p. 431.
[3] S.K. Bhargava, J. Tardio, J. Prasad, K. Foger, D.B. Akolekar, S.C. Grocott, Ind. Eng. Chem. Res. 45 (2006) 1221.
[4] F. Larachi, Topics Catal. 33 (2005) 109.
[5] F. Arena, R. Giovenco, T. Torre, A. Venuto, A. Parmaliana, Appl. Catal. B 45 (2003) 51.
[6] F. Arena, E. Alongi, P. Famulari, A. Parmaliana, G. Trunfio, Catal. Lett. 107 (2006) 39.
[7] F. Arena, J. Negro, A. Parmaliana, L. Spadaro, G. Trunfio, Ind. Eng. Chem. Res. 46 (2007) 6724.
[8] M. Abecassis-Wolfovich, M.V. Landau, A. Brenner, M. Herskowitz, J. Catal. 247 (2007) 201.
[9] A.M.T. Silva, R.R.N. Marques, R.M. Quinta-Ferreira, Appl. Catal. B 47 (2004) 269.
[10] H. Chen, A. Sayari, A. Adnot, F. Larachi, Appl. Catal. B 32 (2001) 195.
[11] S. Hamoudi, F. Larachi, A. Sayari, J. Catal. 177 (1998) 247.
[12] S.T. Hussain, A. Sayari, F. Larachi, Appl. Catal. B 34 (2001) 1.
[13] F. Arena, A. Parmaliana, G. Trunfio, Stud. Surf. Sci. Catal. 172 (2007) 489.
[14] M. Abecassis-Wolfovich, R. Jothiramalingam, M.V. Landau, M. Herrskowitz, B. Viswanathan, T.K. Varadarajan, Appl. Catal. B 59 (2005) 91.
[15] M. Abecassis-Wolfovich, M.V. Landau, A. Brenner, M. Herskowitz, Ind. Eng. Chem. Res. 43 (2004) 5089.
[16] F. Arena, G. Trunfio, J. Negro, B. Fazio, L. Spadaro, Chem. Mater. 19 (2007) 2269.
[17] F. Arena, G. Trunfio, J. Negro, L. Spadaro, Mater. Res. Bull. 43 (2008) 539.
[18] G. Blanco, M.A. Cauqui, J.J. Delgado, A. Galtayries, J.A. Perez-Omil, J.M. Rodriguez-Izquierdo, Surf. Interf. Anal. 36 (2004) 752.
[19] S.T. Hamoudi, A. Sayari, F. Larachi, J. Catal. 201 (2001) 153.
[20] G.-Y. Adachi, T. Masui, in: A. Trovarelli (Ed.), Catalysis by Ceria and Related Materials, vol. 3, Imperial College Press, London, UK, 2002, p. 51.
[21] F. Arena, T. Torre, C. Raimondo, A. Parmaliana, Phys. Chem. Chem. Phys. 3 (2001) 1911.
[22] J. Wang, W. Zhu, S.Z. Yang, W. Wang, Y. Zhou, Appl. Catal. B 78 (2008) 30.
[23] A. Bielañski, J. Haber, Oxygen in Catalysis, Marcel Dekker, Inc., New York, 1991.